AIAA JOURNAL
Vol. 49, No. 6, June 2011

Transonic Aeroelastic Instability Searches Using Sampling and Aerodynamic Model Hierarchy

S. Timme* and K. J. Badcock†
University of Liverpool, Liverpool, England L63 3GH, United Kingdom

DOI: 10.2514/1.J050509

A hierarchy of flow models is exploited for transonic aeroelastic stability analysis using the kriging interpolation technique applied within the Schur complement eigenvalue framework. In the Schur framework, a modified structural eigenvalue problem describes the coupled aeroelastic system with a precomputed interaction term depending on the response frequency. The interaction term, representing the influence of the high-dimensional computational fluid dynamics system, is approximated by reconstruction based on samples that can be computed using a frequency or time domain solver. The computationally cheap approximation model is developed and discussed in this paper for two-degree-of-freedom aerofoil cases. The approximation model is used for both the parametric blind search of aeroelastic instability and for updating predictions based on aerodynamic models of different fidelities.

Nomenclature

A	=	Jacobian matrix
F	=	regression matrix
$\boldsymbol{f}$	=	vector with regression basis functions
I	=	identity matrix
i	=	imaginary unit ($\sqrt{-1}$)
M_r	=	freestream Mach number
$\mathcal{N}$	=	normal distribution
n	=	number of normal modes/number of unknowns
$\boldsymbol{p}$	=	eigenvector
R	=	correlation matrix
$\boldsymbol{R}$	=	residual vector
$\boldsymbol{r}$	=	correlation vector
Re	=	chord Reynolds number
S	=	Schur complement matrix
$\boldsymbol{s}$	=	vector with sample parameter location
S^c	=	interaction term of Schur complement matrix
$\hat{S}^c$	=	kriging approximation of Schur interaction term
$\bar{u}$	=	reduced velocity
V	=	flutter speed index ($\bar{u}/\sqrt{\mu_s}$)
$\boldsymbol{w}$, $\dot{\boldsymbol{w}}$	=	vector of unknowns and corresponding temporal derivatives
$\boldsymbol{x}$	=	vector with unsampled location
$\boldsymbol{y}$	=	solution vector of linear system
$\boldsymbol{y}_s$	=	vector with sampled system output
$\boldsymbol{\alpha}_k$	=	vector of Fourier coefficients for fluid response
$\boldsymbol{\beta}$	=	vector of regression parameters
$\boldsymbol{\beta}_k$	=	vector of Fourier coefficients for structural forcing
λ	=	eigenvalue
μ	=	independent/bifurcation parameter
μ_s	=	aerofoil-to-fluid mass ratio
σ	=	eigenvalue real part
σ	=	standard deviation
φ	=	matrix of standard errors in kriging prediction
ω	=	eigenvalue imaginary part/circular frequency

Subscripts

F	=	critical/instability point
f	=	fluid
s	=	structural
ε	=	small variation
0	=	steady-state/mean value

Presented as Paper 2010-3048 at the 51st AIAA/ASME/ASCE/AHS/ASC Structures, Structural Dynamics, and Materials Conference, Orlando, FL, 12–15 April 2010; received 2 March 2010; revision received 15 March 2011; accepted for publication 15 March 2011.

*Research Associate, Computational Fluid Dynamics Laboratory, School of Engineering; Sebastian.Timme@liverpool.ac.uk. Member AIAA.

†Professor, Computational Fluid Dynamics Laboratory, School of Engineering; K.J.Badcock@liverpool.ac.uk. Senior Member AIAA.

I. Introduction

A CAPABILITY missing from the nonlinear aerodynamic modeling tools available for aeroelasticity is a general method to update lower-fidelity models with better information as it becomes available. Simple parameterized models are used in structural dynamics to facilitate this type of analysis [1], and experiments are exploited to tune the parameters to match observations. The sensitivity to parameters can be easily assessed. In aerodynamics using linear tools in the frequency domain, such as the doublet lattice method, various approaches have been discussed in the literature focusing on correcting the aerodynamic influence coefficient matrix with nonlinear data [2]. When nonlinear flow models are concerned, there are no well established methods for exploiting measured data or higher-fidelity predictions. In addition, aeroelastic applications often describe high-dimensional parametric problems comprising 10s of 1000s of possible test points and flight conditions [3–5]. Efficiency in predicting the most critical conditions to assist in flight testing is paramount. The current paper describes an investigation into developing a method that will address these points by applying computational fluid dynamics (CFD) for the limited case of transonic aeroelastic predictions for two-degree-of-freedom aerofoils.

Transonic aerodynamics introduce nonlinearity into the aeroelastic dynamics (while structural nonlinearity is perfectly common as well). Two aeroelastic phenomena are particularly associated with the nonlinear flowfield. One is the transonic dip, where the presence of shock waves reduces the stability of the aeroelastic system. The second is limit-cycle oscillation (LCO), where the limiting mechanisms of the amplitude of the dynamic response are shock motions and separation. In [6], for instance, the influence of aerodynamic modeling assumptions on the amplitude of a store-induced LCO was investigated for the Goland wing. The dependence of LCO amplitudes on the modeling level, considering both inviscid and viscous flows, was discussed. It was argued that shock/boundary-layer interaction in this case causes trailing-edge separation and retards the shock movement (substantial in the inviscid case

otherwise), thus limiting the LCO amplitude. Modeling both the inviscid/viscous interaction as well as the extent of the shock-induced separated regions is therefore important.

The stability of an aeroelastic system can be inferred from time-accurate simulations following an initial excitation of the system, even though the appearance of subcritical LCO can complicate this interpretation. Calculations of complete aircraft configurations have been made [7,8]. The time-accurate approach is very capable due to its generality. However, the significant computational cost (in particular, to solve for the unsteady nonlinear transonic aerodynamics) is a major drawback of this approach. A requirement to search a space of system parameters and flight conditions for critical conditions makes this situation worse. The issue of cost generally limits the analysis to a few carefully chosen cases. Alternative approaches have been investigated to obviate the computational cost and to permit routine calculations over larger parameter ranges [9]. One popular method is reduced-order modeling (ROM) based on proper orthogonal decomposition (POD). For a robust and reliable ROM to exist, the parameter space and flow phenomena of interest have to be covered by the set of system responses used to establish the ROM; thus, creating the large number of system responses is the main cost. In addition, the reliability of the POD/ROM approach under parameter changes is a topic of investigation [10]. A variant of the POD technique was applied to both deal with incomplete data in the reconstruction of aerodynamic flowfields and to provide a link in updating numerical predictions with experimental measurements [11].

An alternative approach discussed in the present work uses the theory of dynamical systems to predict aeroelastic instability of the Hopf type commonly leading to flutter or LCO. Here, a stability problem for a steady-state solution of the aeroelastic system is examined instead of performing unsteady simulations. Stability is lost by a Hopf bifurcation when a pair of complex conjugate eigenvalues of the system Jacobian matrix crosses the imaginary axis for some value of a critical system parameter. Following an approach first published in [12,13], the bifurcation method was successfully tested on a two-dimensional aerofoil configuration, free to move in pitch and plunge. Convergence problems associated with applying a direct solver to a large linear system were resolved by using an iterative sparse linear solver [14]. The method was extended to a larger problem investigating the AGARD 445.6 wing using a modal structural model [15]. Later, the shifted inverse power method was adapted to allow tracing of the critical eigenvalues with changing values of the system parameter. This provides information about damping and frequency of the aeroelastic modes [16]. Also, a model reduction technique based on the center manifold theory was investigated to simulate an LCO response in the vicinity of the linear instability point [16].

An improved version of the basic method used a Schur complement eigenvalue formulation to enhance computational performance [17]. It was applied to several wing structures and complete aircraft configurations to study uncertainty in the predicted instability due to structural variability [18]. This approach views the coupled system as a modified structural eigenvalue problem with the interaction (correction) term, which depends on the response frequency, being precomputed. In the current paper, the approximation of this interaction term is formulated so that the stability problem can be solved efficiently in larger parameter spaces. In addition, it allows that a hierarchy of aerodynamic models can be exploited, with cheaper models being used to evaluate possible conditions of interest for more expensive models, the evaluation of which is then used to update the approximation.

The paper continues with the formulation and benchmarking of the aerodynamic and aeroelastic tools. The generation of the interaction term and its approximation using the kriging interpolation technique are then considered, and an aeroelastic stability analysis for a pitch and plunge aerofoil is presented to illustrate the approach. Finally, ideas for coordinated sampling and model updating to assist the construction of the approximation model applied in aeroelastic stability analysis and to allow parametric instability searches are investigated for the aerofoil model.

II. Eigenvalue Stability Analysis Using Computational Fluid Dynamics

A. Flow and Structural Models

In [19], four main aerodynamic modeling levels are discussed: linear and nonlinear potential, Euler, and Navier–Stokes. The physics in the simulation can be built up from linear potential flow. The nonlinear potential model adds nonlinear compressible flow effects. The Euler equations add entropy and vorticity effects, while the Navier–Stokes equations include viscous and heat-conduction effects. For aerodynamic flows of practical interest, the Reynolds-averaged form of these equations (RANS) is generally used, introducing the requirement for turbulence models. In the current paper, the RANS equations, the Euler equations, as well as the unsteady nonlinear full potential equations, with and without coupling of an integral boundary-layer model, are considered as aerodynamic models in the context of aerofoil stability analysis.

The RANS and Euler equations are solved using an established research code [20]. Basic features of the code include a spatial discretization done by a block-structured cell-centered finite volume scheme, where implicit time marching is applied for steady-state solves, and a (implicit) second-order dual time stepping is used for unsteady simulations [21]. Convective fluxes are evaluated by the approximate Riemann solver of Osher and Chakravarthy [22], with the MUSCL scheme [23] achieving essentially second-order accuracy and van Albada's limiter preventing spurious oscillations around steep gradients. Viscous fluxes are evaluated, making use of the Green–Gauss theorem. Boundary conditions are enforced using two layers of halo cells. The shear-stress transport k-ω turbulence model [24] used in this work is solved in a fashion similar to the RANS equations, with the source term evaluated at cell centers.

The continuity and Bernoulli equations constitute the unsteady full potential model (FP) solved by a newly developed research code [25]. Basic features of the code include a spatial discretization done by an unstructured triangular vertex-based finite volume scheme, where Newton's iterative method is applied for steady-state solves and the preceding second-order dual time stepping is used for unsteady simulations. The convective fluxes are evaluated by a second-order upwind scheme using a linear least-squares reconstruction. The potential jump at the aerofoil trailing edge (i.e., circulation) to satisfy the Kutta condition is convected downstream in the usual unsteady fashion [26]. Boundary conditions are set using a layer of halo vertices with a transpiration boundary condition applied at solid walls. Viscous effects (FPV) are modeled using an integral boundary-layer approach [27–30]. Wall blowing is applied to model

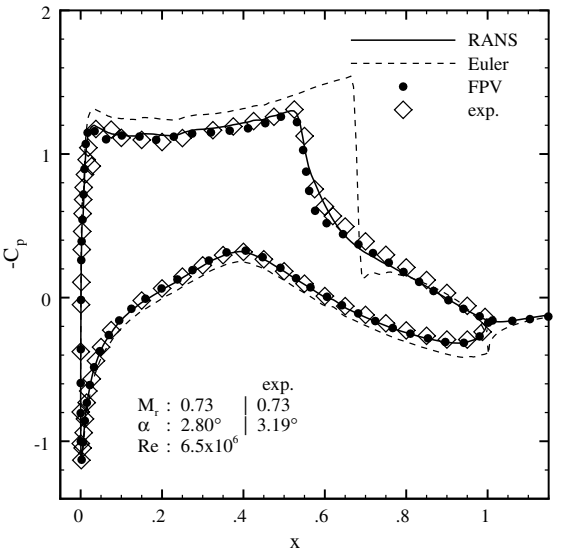

Fig. 1 Pressure distribution of RAE 2822 aerofoil case 9 showing comparisons of measurements as presented in [32] and simulations using RANS, Euler, and FPV.

the leading-order effect of the viscous layer, displacing the outer inviscid flow by a distance equal to the displacement thickness [31].

Results for one standard test case are presented to build confidence in the developed full potential flow solver. Steady measurements of pressure distributions in subsonic and transonic flow regimes are given in the experimental database of [32] for the supercritical Royal Aircraft Establishment (RAE) 2822 aerofoil. Results are shown in Fig. 1 for transonic case 9. As the simulations assume free flight, the numerical flow conditions were adjusted to match the experiments subject to wall interference effects. Experimental data and viscous simulations are in good agreement. The inviscid FP simulations did not converge due to the strength of the shock wave significantly violating the full potential modeling assumptions.

The structure in the aeroelastic problem is described by the dynamics of a two-degree-of-freedom aerofoil, as found in the standard literature on aeroelasticity [33,34]. The aerofoil with oscillating pitching and plunging motion represents the torsional and bending behaviors of a wing structure. The linear model is idealized as a point mass located at the center of gravity, as well as a torsional and a translational spring attached to the elastic center located some distance away from the center of gravity. Details on the specific model applied are given, for instance, in [12,14].

B. Original Schur Eigenvalue Method

Write the aeroelastic system as $\dot{\boldsymbol{w}} = \boldsymbol{R}(\boldsymbol{w}, \mu)$, where the vector of unknowns $\boldsymbol{w}$ contains fluid and structural contributions and $\boldsymbol{R}$ is the corresponding residual vector. The system depends on an independent parameter μ representing, for instance, dynamic pressure or altitude. An equilibrium solution $\boldsymbol{w}_0$ of the nonlinear system satisfies $\boldsymbol{R}(\boldsymbol{w}_0, \mu) = 0$. The theory of dynamic systems gives criteria for an equilibrium to be stable. In particular, stability is determined by eigenvalues, $\lambda = \sigma \pm i\omega$, of the system Jacobian matrix $A(\boldsymbol{w}_0, \mu)$ evaluated at the steady-state and chosen values of μ. A stable system has all its eigenvalues with a negative real part, while in many aeroelastic applications, a pair of complex conjugate eigenvalues with zero real parts defines the onset of an instability of the Hopf type leading to flutter and LCO. Linear stability is predicted by solving the standard eigenvalue problem $A\boldsymbol{p} = \lambda\boldsymbol{p}$, where the Jacobian matrix is partitioned in blocks expressing the different dependencies:

$$A = \frac{\partial \boldsymbol{R}}{\partial \boldsymbol{w}} = \begin{pmatrix} A_{ff} & A_{fs} \\ A_{sf} & A_{ss} \end{pmatrix} \tag{1}$$

For convenience, the eigenvector $\boldsymbol{p}$ is partitioned into unknowns corresponding to fluid and structural contributions [17]. Then, the Schur complement eigenvalue method is given as $S(\lambda)\boldsymbol{p}_s = \lambda\boldsymbol{p}_s$, defining a small nonlinear eigenvalue problem. The Schur complement matrix $S(\lambda)$ is explicitly written as

$$S(\lambda) = A_{ss} - A_{sf}(A_{ff} - \lambda I)^{-1}A_{fs} \tag{2}$$

where the first term on the right-hand side defines the structural eigenvalue problem, while the second part constitutes the interaction (coupling) term $S^c = -A_{sf}(A_{ff} - \lambda I)^{-1}A_{fs}$. To solve this complex-valued eigenvalue problem for the unknowns $[\mathbf{p}_s^T, \lambda]^T$, the system is augmented for scaling the structural eigenvector $\boldsymbol{p}_s$ against a real-valued constant vector. While the standard eigenvalue problem has $n_f + 2n + 1$ unknowns, the Schur formulation only has $2n + 1$ where the number n of relevant (structural) normal modes is generally small compared with the dimension n_f of the fluid system. There are several ways to evaluate the roots of the Schur residual (i.e., the augmented system), as outlined in the following and with more details given in [17,18].

An efficient way of finding the roots of nonlinear systems are variants of Newton's methods, which require forming the residual and its Jacobian matrix. The main cost in either method is to evaluate the interaction term S^c, as it includes operations on the high-dimensional fluid system, whereas the cost to form the structural Jacobian matrix A_{ss} is negligible. Using the exact Newton's method, the interaction term in the Schur residual is evaluated by first forming the product $A_{fs}\boldsymbol{p}_s$ for the current approximation to the eigenvector and then solving one linear system, $(A_{ff} - \lambda I)\boldsymbol{y} = A_{fs}\boldsymbol{p}_s$, the solution of which is multiplied with the matrix A_{sf}. Applying finite differences gives the Schur Jacobian matrix where multiple evaluations of the residual are required. Resulting linear systems are solved using a preconditioned Krylov subspace iterative method [16] in the structured multiblock code, while a direct solver [35] is applied in the unstructured code.

As there are n relevant solutions of the nonlinear eigenvalue problem, the cost of forming the interaction term at each Newton iteration for each value of the independent parameter becomes too high without approximations. To overcome this, a series approximation [36] of the Schur complement matrix can be written for $\lambda = \lambda_0 + \lambda_\varepsilon$ as

$$\begin{aligned} S(\lambda) \approx A_{ss} - A_{sf}[&(A_{ff} - \lambda_0 I)^{-1} \\ &+ \lambda_\varepsilon(A_{ff} - \lambda_0 I)^{-1}(A_{ff} - \lambda_0 I)^{-1}]A_{fs} \end{aligned} \tag{3}$$

where λ_ε is a small variation to a reference λ_0, obtained from a normal mode frequency or a previously converged solution. Precomputing the factors in the series for the right-hand side matrix A_{fs} (requiring $4n$ linear solves per reference λ_0) and storing their projection onto the structural system (using the matrix A_{sf}) allows the application of the expansion in the vicinity of λ_0. Two approaches have been discussed. The quasi-Newton method evaluates the (exact) residual by the nonlinear approach given in the previous paragraph, while the series is used for the Schur Jacobian matrix. The series method also applies the series expansion to the residual, which is possible for small λ_ε and for an independent parameter μ not affecting the precomputed values.

In this work, as discussed in the next section, a new method is introduced. The Schur residual and the Jacobian matrix are formed by approximating the interaction term S^c by a reconstruction based on samples (i.e., exact evaluations of this term) covering the parameter space of interest.

III. Approximate Schur Eigenvalue Method

The elements of the Schur interaction matrix are a function of the eigenvalue, particularly the response frequency, and the parameters of the steady-state simulation, including parameters in both the structural and aerodynamic models. While the full-order approximations of the Schur eigenvalue method described previously (i.e., quasi Newton and series) have been used extensively for large-scale problems [17,18], it is clear that neither of these approaches is appealing when (high-dimensional) parametric searches for instability are desired. Evaluating the interaction matrix S^c based on the full-order approximations accounts for the highest cost in the stability analysis, as operations on the CFD fluid system are constantly required, making the approach prohibitive for parametric searches. Instead, for computationally expensive tasks (such as evaluating the interaction matrix), it is common to generate a cheap approximation (surrogate model) based on relatively few runs of the expensive model to provide information about its response at untried parameter combinations. Once an approximation based on full-order samples is evaluated, the stability problem is solved without relying on the exact solver becoming very cheap.

Two approximations are used in the current work. First, the interaction matrix is evaluated for an eigenvalue with zero real part, while the small nonlinear eigenvalue problem is still solved for an eigenvalue having a nonzero real part. In this sense, it is an analogy to the conventional p-k method [37], with the aerodynamic influence evaluated assuming constant amplitude harmonic motion. Second, the variation of the interaction matrix in the parameter space required for the stability analysis is found from interpolation of exact samples. Then, the eigenvalue problem is written as

$$[A_{ss} + \hat{S}^c(\omega)]\boldsymbol{p}_s = \lambda\boldsymbol{p}_s \tag{4}$$

where $\hat{S}^c$ denotes the approximation of S^c. More interesting, for the two-degree-of-freedom aerofoil discussed in the present study, the interaction term S^c is independent of the bifurcation parameter,

chosen to be the reduced velocity $\bar{u}$, thus simplifying the discussion. At the critical eigenvalue $\lambda_F = i\omega_F$ (i.e., the linear instability point), the approximation of constant amplitude harmonic motion is exact within the limits of the interpolation algorithm.

Using this approach, the two main tasks of the stability analysis are an appropriate sampling of the parameter space to describe the important physics accurately and a robust interpolation of these samples. Methods to evaluate exact samples of the interaction matrix are given next, while sampling techniques for parametric searches will be discussed in a separate main section. Different sampling techniques will be presented together with results for an aerofoil test case. The method of choice in this work for the task of interpolation is kriging, described in Sec. III.B, while other interpolation techniques can be just as effective.

A. Generating Samples

The interaction matrix can be formed in both the frequency and time domains. Solving the $2n$ linear systems (one for each column of the matrix A_{fs}) against the fluid system directly and multiplying with the matrix A_{sf} to form the Schur interaction matrix is referred to as the linear frequency domain approach. In the time domain, the most common approach is to run forced modal motion simulations and to decompose the resulting unsteady generalized forces (i.e., lift and moment coefficients in the case of the aerofoil structural model) in a Fourier series. These coefficients are then divided by the corresponding Fourier coefficients of the excitation signal to give the elements of the interaction matrix.

Alternatively, the interaction matrix is evaluated from a Fourier analysis of the unsteady responses in individual control volumes of the fluid mesh. To show this, the vector of unknowns is rearranged as the sum of a steady-state solution $\boldsymbol{w}_0$ and a corresponding unsteady perturbation $\delta\boldsymbol{w}$. Writing the fluid part of the aeroelastic system in its time-linearized form,

$$\dot{\boldsymbol{w}}_f = A_{ff}\delta\boldsymbol{w}_f + A_{fs}\delta\boldsymbol{w}_s \tag{5}$$

with the Jacobian matrix blocks A_{ff} and A_{fs} evaluated at the steady state, and expressing the unsteady perturbation of the fluid and structure in a truncated exponential Fourier series [38], the following expression can be given:

$$\sum_{k=-K}^{K} \boldsymbol{\alpha}_k = -\sum_{k=-K}^{K} (A_{ff} - ik\omega I)^{-1} A_{fs}\boldsymbol{\beta}_k \tag{6}$$

The complex-valued vectors of Fourier coefficients ($\boldsymbol{\alpha}_k$ for fluid response in control volumes and $\boldsymbol{\beta}_k$ for structural forcing) are evaluated from the time signal over a period $T = 2\pi/\omega$ (with ω as the fundamental frequency). After multiplying with the matrix block A_{sf} (evaluated analytically or by finite differences), the expression in Eq. (6) corresponds to the interaction term for an undamped eigenvalue, with column and magnitude set by the applied structural forcing.[‡] Evaluating the Fourier coefficients at integer multiples k of the fundamental frequency (provided the system was excited accordingly) gives the interaction matrix at these discrete frequencies.

Solutions of the fully nonlinear system $\dot{\boldsymbol{w}}_f = \boldsymbol{R}(\boldsymbol{w}_f, \boldsymbol{w}_s)$ approach the time-linearized results if the amplitude of the forced motion is sufficiently small (i.e., the unsteadiness in the flow is linearly dependent on the structural motion). The step of using the nonlinear system is required if the Jacobian matrices in Eq. (5) for the fluid contribution are not available explicitly (otherwise, the linear frequency domain approach should be used).

B. Kriging/Cokriging Technique

In the kriging interpolation technique, the deterministic response of a simulation is treated as a realization of a stochastic process where the kriging predictor, written at an unsampled location $\boldsymbol{x}$ as

$$\hat{y}(\boldsymbol{x}) = \boldsymbol{f}(\boldsymbol{x}) \cdot \boldsymbol{\beta} + \boldsymbol{r}(\boldsymbol{x}) \cdot [R^{-1}(\boldsymbol{y}_s - F\boldsymbol{\beta})] \tag{7}$$

is composed of a low-order regression model and a random normally distributed signal with zero mean and a covariance depending on the variance of the input samples and the correlation between two parameter locations. Thus, the second term (the error term) is not independent at different locations but is related to the distance between points in the parameter space. The latter expression is given for a single scalar output y, the sampled system responses of which are contained in the vector $\boldsymbol{y}_s$, while its multidimensional extension is straightforward. The vectors $\boldsymbol{f}$ and $\boldsymbol{r}$ contain the regression basis functions and the correlation of location $\boldsymbol{x}$ with the provided samples, respectively, while the matrices F and R are formed by applying the corresponding vectors to the samples. The vector of regression parameters $\boldsymbol{\beta}$ is the generalized least-squares estimator of the overdetermined regression problem $\boldsymbol{y}_s \approx F\boldsymbol{\beta}$. The parameters of the computationally cheap kriging model are determined for a provided set of numerical samples of the full-order formulation with the critical step of finding the optimal parameters for the correlation [39,40]. Besides the prediction of a function, kriging also provides the (mean squared) error of the prediction that, importantly, vanishes at a sampled location interpolating the exact system response. Details on the specific kriging toolbox used in this work can be found in [41]. Previously, the kriging approximation was used for generating aerodynamic data applied in flight dynamics studies [42].

A representative element of the interaction matrix is shown in Fig. 2 for the four aerodynamic models discussed in this work. The element describes the response in the plunge degree of freedom due to a disturbance in the plunge rate for the NACA 0012 "heavy case" aerofoil configuration, the structural parameters of which are given in [14]. In the figures, the open circles indicate sample points, while the meshed surfaces describe the response as given by the kriging interpolation. The samples were extracted using either the linear frequency domain or, for the RANS simulations, the time domain approach with a dimensionless excitation amplitude of 7.75×10^{-3} applied. The fewer RANS samples reflect the higher cost, not only using the highest modeling level, but also requiring sample generation in the time domain (as a frequency domain, the RANS solver is currently not available). To illustrate the important part of the two-dimensional parameter space, using response frequency and the freestream Mach number, the trace of the instability boundary is projected onto the surfaces. Inspecting the figures, interesting observations can be made. Note that similar response surfaces were found for the remaining elements of the interaction matrix.

To start with, it is found that the different flow models produce similar response features, which should be expected, as the shock dominated physics are included in all flow descriptions, while separation is not yet an important factor in the considered Mach number range. In the subsonic range, the aerodynamic influence has small variations with changing system parameters, while in the transonic range, clear variations (in particular, with respect to the freestream Mach number) are present. One distinct difference is found for the FP flow model at the higher Mach numbers and lower frequencies. Here, the imaginary part of the shown element takes on values almost double the elements of the other models, which is probably due to the shock dynamics (including location and strength) being incorrectly predicted. This suggests that, once the correct response features are simulated reasonably well by models of different fidelity, a hierarchy of flow models can be exploited in the stability analysis by combining cheaper response evaluations with available better (more expensive) information.

In the discussion of kriging tools, such similar (correlated) trends in response surfaces can be exploited. Cokriging techniques use additional information on the functional behavior of the response, such as gradients or correlated covariables. Using a spatially correlated, cheaper (usually), and hence densely sampled covariable to augment the input parameter space of a (usually) more expensive, sparsely sampled primary variable allows the accurate prediction of the primary variable with very few samples. This can be formulated by writing the dependence of a high-fidelity (hf) sample as $y_s^{\mathrm{hf}} = y_s^{\mathrm{hf}}(\boldsymbol{s}, y_s^{\mathrm{lf}})$, where $\boldsymbol{s}$ denotes the sample parameter location and

[‡]In this sense, the matrix block A_{sf} integrates the individual fluid responses, which makes it equivalent to using the (integrated) generalized forces.

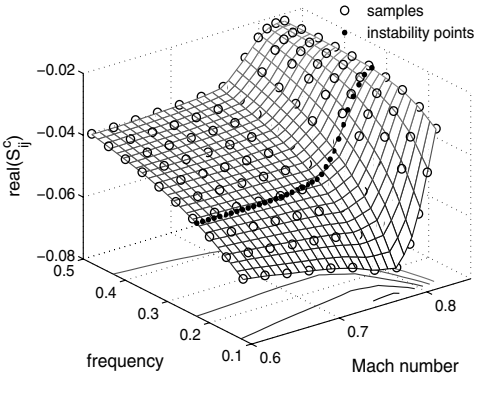

a) FP – real part

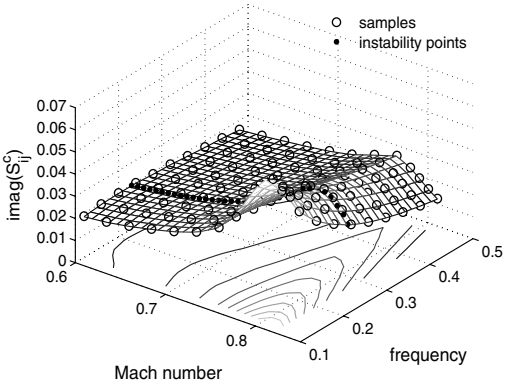

b) FP – imaginary part

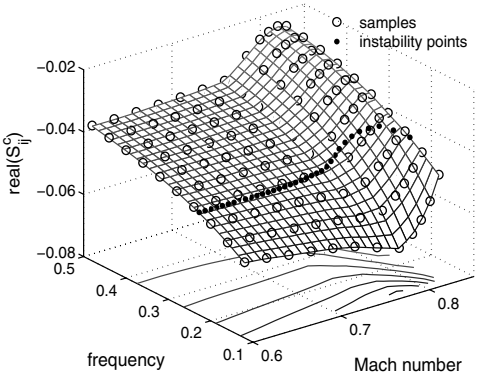

c) FPV – real part

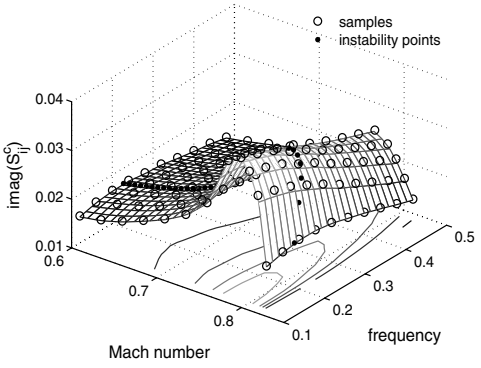

d) FPV – imaginary part

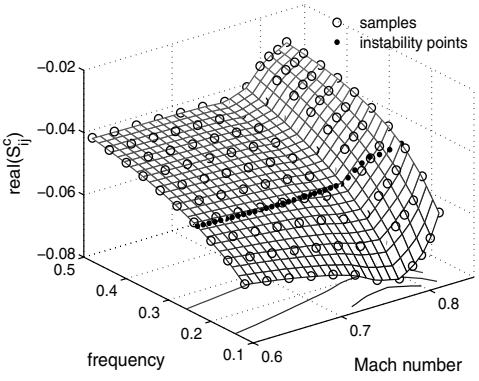

e) Euler – real part

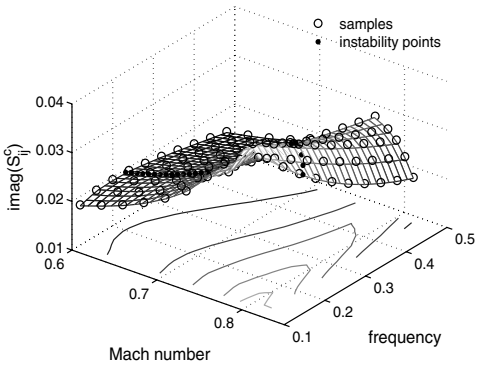

f) Euler – imaginary part

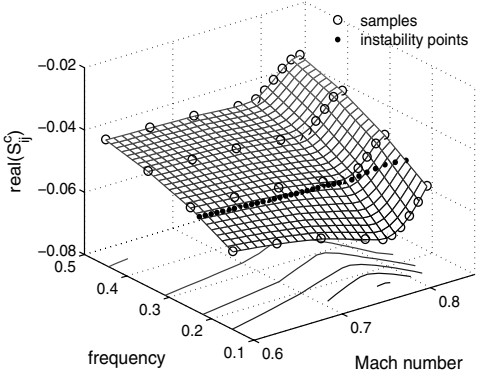

g) RANS – real part

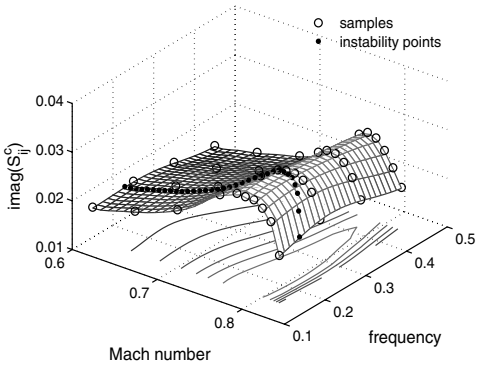

h) RANS – imaginary part

Fig. 2 Extracted and interpolated element S_{33}^c for NACA 0012 aerofoil configuration using four aerodynamic models.

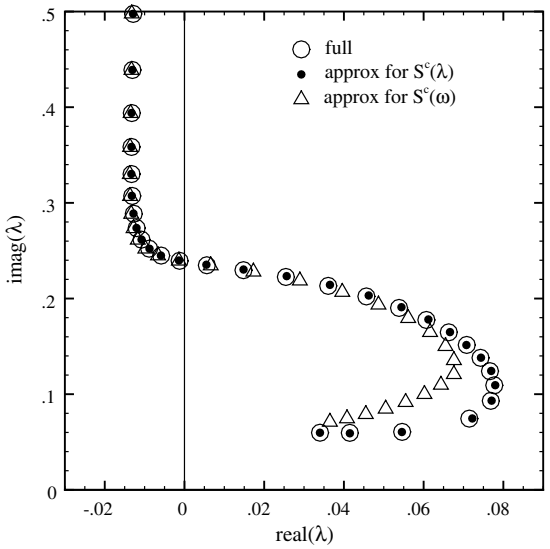

Fig. 3 Mode tracing at Mach 0.7 for NACA 0012 aerofoil configuration using Euler flow model and comparing results using full-order and kriging approximated interaction matrix; approximation for eigenvalues with nonzero real part $S^c(\lambda)$ and zero real part $S^c(\omega)$.

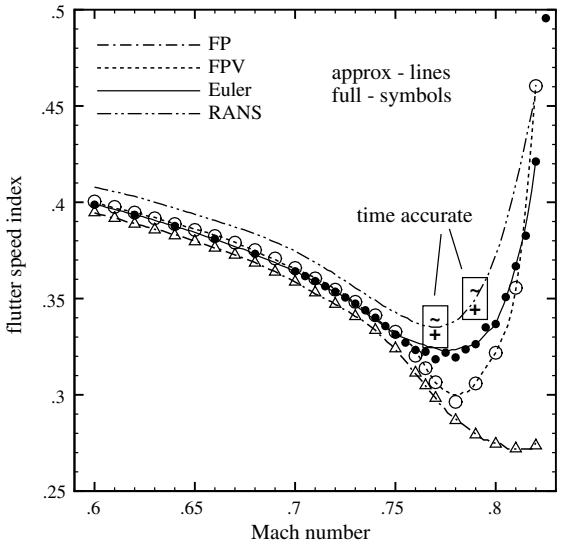

Fig. 4 Critical flutter speed index for NACA 0012 aerofoil configuration using four aerodynamic models and showing comparison of full-order (full) and approximation models (approx).

y_s^{lf} is the correlated lower-fidelity (lf) output. A standard kriging model can then be applied. The cheaper model provides a trend of the system response, with the higher-fidelity data updating the prediction [40]. In this context, the cheaper model is established by either a lower level aerodynamic modeling (which exploits the aerodynamic hierarchy of flow models) or by a higher level model solved on a coarse grid. This will be applied in Sec. V.B.

IV. Results for Aerofoil Test Case

The use of the response surfaces presented previously is now discussed for stability analysis. Figure 3 shows the tracing with respect to the reduced velocity of the lower-frequency aeroelastic mode for the NACA 0012 heavy case aerofoil configuration using the Euler flow model only. The calculation of 60 points on the root locus took less than 1 s of CPU time applying the kriging approximation, whereas the full formulation having a grid with 15,000 control volumes took more than 1 h (about 1 min per point) on a modern desktop personal computer using the quasi-Newton method.

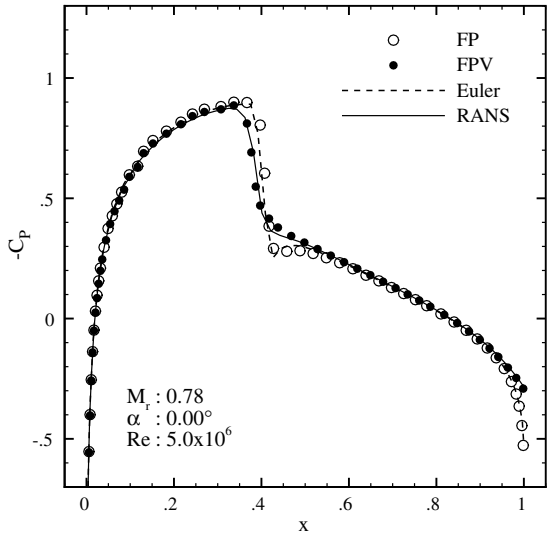

Fig. 5 Pressure coefficient for NACA 0012 aerofoil and different flow models.

Unsteady time marching at an individual reduced velocity (with a dimensionless time step of 0.05) takes about 13 min per cycle of motion (comprising about 500 steps). Two approximation models are shown. One used exact samples $S^c(\omega)$ with zero damping and a varying frequency, whereas the second one was constructed for both varying damping and frequencies to have samples $S^c(\lambda)$. Using the latter approximation, the trace of the relevant eigenvalue follows the full-order reference prediction precisely. However, the eigenvalue can be traced quite accurately, even away from the imaginary axis, for samples assuming constant amplitude harmonic motion. The error introduced by the approximation $S^c(\omega)$ is very small in the relevant region close to the imaginary axis, suggesting that the variation of the elements in the interaction matrix with damping (or at least that the influence of this variation on the eigenvalue problem) is small.

Figure 4 presents the subsonic and transonic instability boundaries as critical values of the flutter speed index $V_F = \bar{u}_F/\sqrt{\mu_s}$ (where μ_s is the aerofoil-to-fluid mass ratio). A comparison of results from the full-order and approximation models is given for the four aerodynamic models. Time-accurate simulations to confirm the RANS predictions (using a chord Reynolds number of 5 million) are included with the plus (tilde) sign indicating a stable (unstable) response due to an initial disturbance in the steady state. The agreement is excellent, as should be expected, since the sample resolution is high, as found in Fig. 2. Remember that the error in the kriging prediction at a sampled location is zero.

The differences in the subsonic regime between the various predictions are small considering the different numerical discretization schemes and flow models, while a slight stabilization of the configuration due to the modeling of viscous effects is observed. Furthermore, it seems that the shock dynamics, which are correctly predicted by the Euler model, act as the dominant mechanism for the aeroelastic instability compared with the viscous effects (in this configuration and for the shown range of Mach numbers). Indeed, shallow separation due to shock/boundary-layer interaction is first encountered at about Mach 0.81 to 0.82. Entering the transonic regime for freestream Mach numbers above 0.73, the differences between full potential (with or without boundary-layer coupling), Euler, and RANS predictions become interesting. While the divergence between FP and FPV results beyond Mach 0.78 are easily explained with the wrong prediction of the shock wave using the inviscid and irrotational FP approach, the difference between FPV and RANS are not. Compared with RANS results, the viscous full potential approach keeps predicting accurate steady flow solutions, as shown in the pressure distribution in Fig. 5. However, it is suggested for the full potential results that the missing physical effects of entropy and vorticity in the transonic regime, which are not captured in the full potential fluid Jacobian matrix, cause the

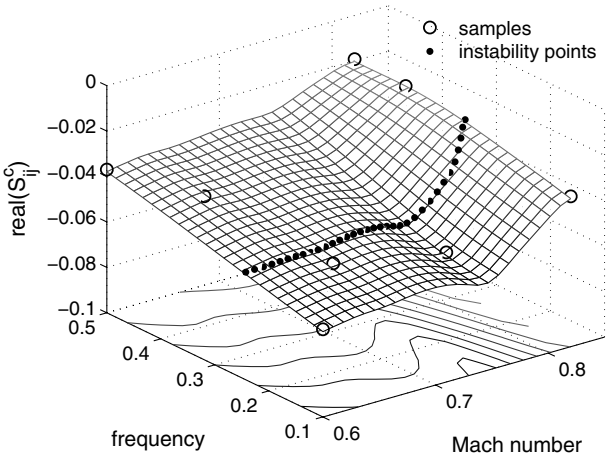

a) Element real (S_{33}^c) for one set of eight samples including trace of instability

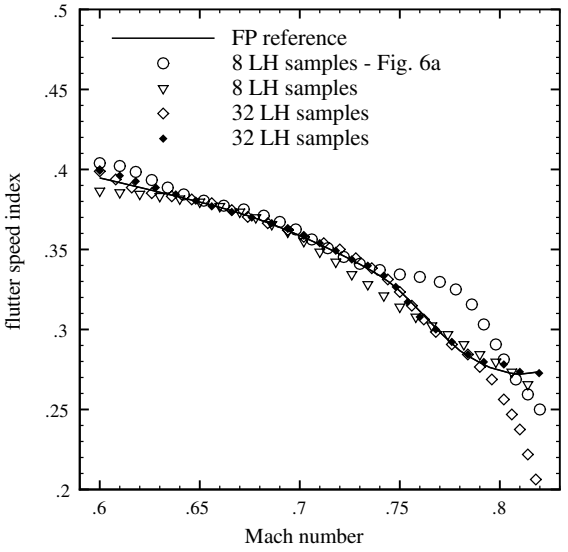

b) Critical flutter speed index compared with reference solution

Fig. 6 LH sampling using FP flow model for NACA 0012 aerofoil configuration.

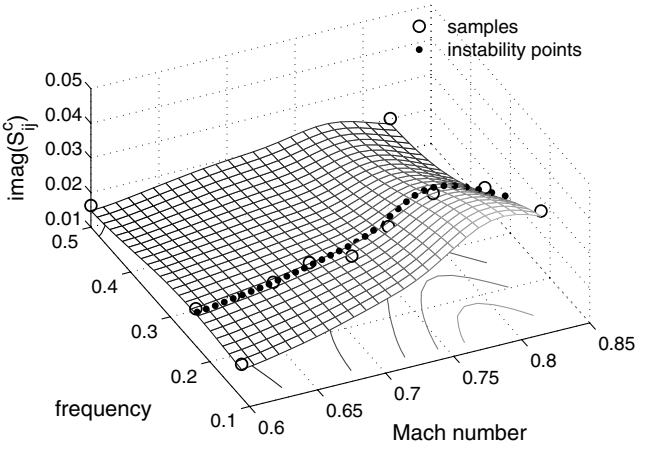

a) Element imag(S_{33}^c) based on 12 samples including trace of instability

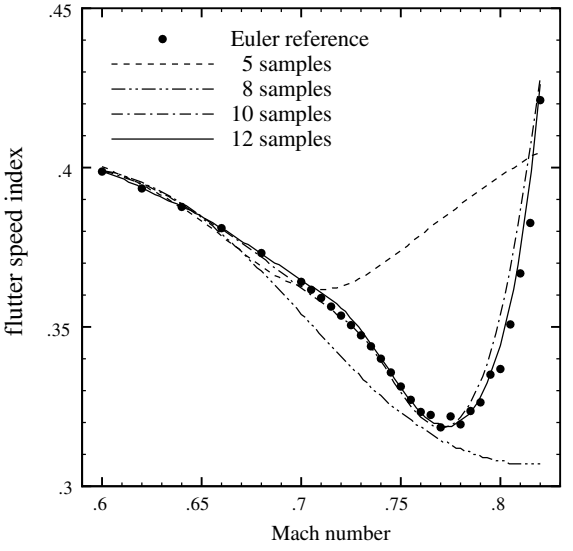

b) Critical flutter speed index compared with reference solution

Fig. 7 Risk-based sampling using Euler flow model for NACA 0012 aerofoil configuration.

underprediction of the instability. More interesting, the introduced errors cause a more conservative stability prediction.

V. Coordinated Sampling and Model Hierarchy

This section first presents different sampling techniques to both arrange the construction of the surrogate model to be computationally more efficient and be aimed at detecting aeroelastic instability in parametric search problems. Then, the updating of aerodynamic models from the hierarchy (using the viscous full potential and the RANS equations) is described. Results for two aerofoil test cases are presented alongside this discussion for the purpose of illustrating the techniques.

A. Coordinated Sampling

The cost to create the approximation (i.e., the number of samples to adequately represent the variation of the interaction matrix) is an important factor in the analysis, especially for an expensive high-fidelity flow model. The large number of uniformly distributed samples as used, for instance, in Fig. 2 does not seem to be required to accurately predict the response surface near the instability. Sampling techniques can be exploited instead. The different techniques presented include Latin hypercube (LH), risk-based, and expected improvement (EI) samplings, details of which are discussed in the following.

LH sampling is considered as an improved version of random sampling [43]. While random sampling creates parameter combinations independently (and possibly without providing additional information), LH sampling ensures that all parts of the parameter space are evenly represented. Therefore, each parameter dimension is divided into a specified number of nonoverlapping bins of equal probability. One sample per dimension is randomly chosen from each bin and then randomly combined with the other parameter dimensions.

This approach is presented in Fig. 6 for the FP flow model using the NACA 0012 aerofoil configuration. Initially, four samples were placed at the corners of the parameter space in each case to avoid extrapolation, while the remaining design points were generated (a priori) by LH sampling. The dimensions of the parameter space are defined to provide a good range for an initial blind search, with the Mach number covering the region of interest (up to mild separation) and the frequency based on typical flutter frequencies (chosen from the structural frequencies). Looking at Fig. 6a, even as few as eight samples can approximate the target reasonably precisely. This observation is supported in Fig. 6b, showing the critical flutter speed index as the true measure for the quality of the approximations while comparing with a reference solution. It is clear that more samples

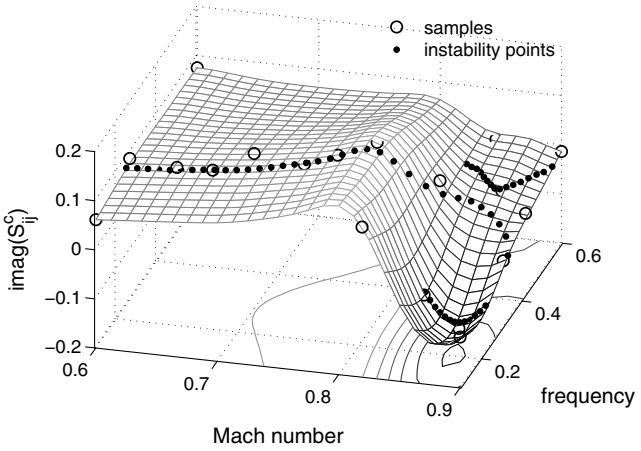

a) Element imag (S^c_{33}) based on 20 samples including trace of instability

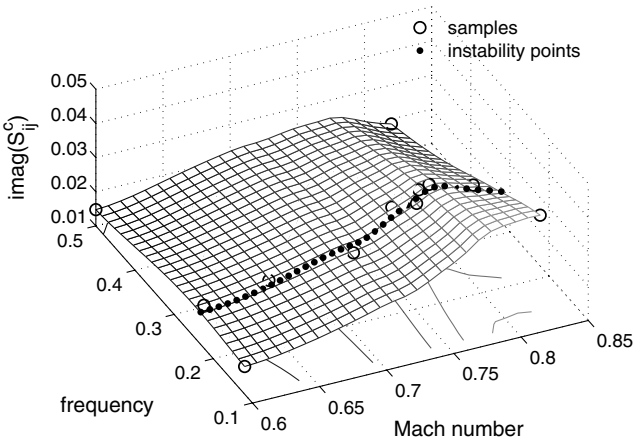

a) Element imag(S^c_{33}) based on 12 samples including trace of instability

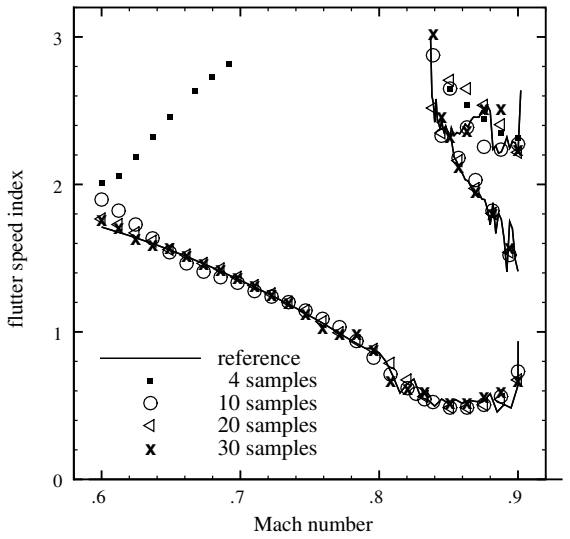

b) Critical flutter speed index compared with reference solution

Fig. 8 Risk-based sampling using Euler flow model for Isogai [44] configuration.

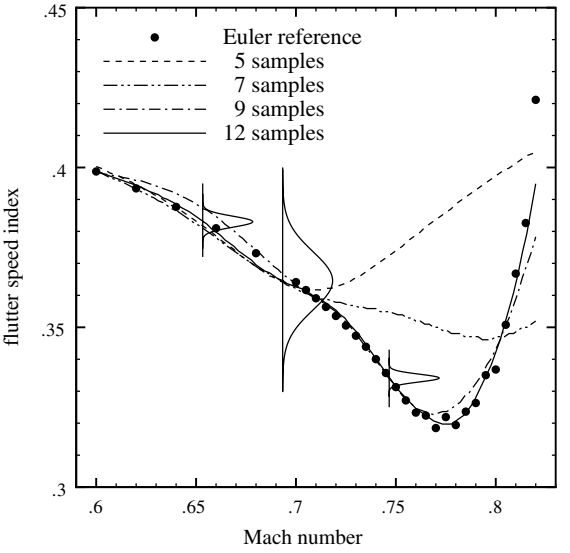

b) Critical flutter speed index compared with reference solution including response probability density functions

Fig. 9 EI sampling using Euler flow model for NACA 0012 aerofoil configuration.

result in a more accurate prediction. However, occasional poor results using different sets of LH samples emphasize the remaining risk of wrong predictions, especially for low numbers of samples, as no information on the target of the approximation (i.e., the predictions of the linear aeroelastic stability limit) is considered.

Looking at Figs. 2 and 6, it was found that many samples are redundant for accuracy in the prediction. As the cost of the stability analysis using the approximation model is very low, it is useful to iteratively perform complete instability searches, always based on the current set of samples, while placing new samples in regions of high risk. Such a risk-based sampling proceeds by first defining an initial search space, in this example, with the four corner points. Then, the relevant aeroelastic modes are traced, and the instability points are predicted. Locating the maximum kriging error (readily available) along the current approximation to the instability boundary gives the new sample location, while other user-predefined criteria are possible. Iterating converges the solution to satisfy user-predefined stopping criteria. This gives some measure of confidence in the prediction in combination with the cost.

The approach is illustrated in Fig. 7 for the NACA 0012 aerofoil configuration using the Euler flow model. It can be seen that new samples are closely placed in the region where they strongly support the prediction. An accurate detection of the instability boundary is quickly obtained. The 10 samples, being sufficient in this example to cover a complete subsonic and transonic regime, correspond to the cost of about 20 steady-state solves (including the simulation of steady flowfields) using the linear frequency domain approach for sample extraction. Evaluating the response surfaces within the entire initial search space is not attempted. As a consequence, mode tracing could become inaccurate further away from the instability, which, however, is a fair tradeoff compared with the cost. If this inaccuracy becomes critical, giving an additional (incorrect) instability in the prediction, the sampling criterion would automatically correct this by placing a new sample.

To give an idea of the computational cost involved having the steady-state solutions available, evaluating 12 samples, requiring $2n$ linear solves per sample in the frequency domain, to cover an entire range of freestream Mach numbers is equivalent to form the series factors in Eq. (3) for the two normal modes of the aerofoil configuration at three individual Mach numbers once, requiring $4n$ linear solves per mode and Mach number. This will become more significant for cases with an increasing number of normal modes.

A second test case is presented using risk-based sampling. The Isogai [44] benchmark case is known to exhibit multiple bifurcations for inviscid flow models in the deep transonic regime. In Fig. 8b, showing the challenging instability boundary, it is found that 10 samples provide a good description of the (inviscid) transonic stability features, while more samples are required to predict the bifurcation points precisely at higher reduced velocities.

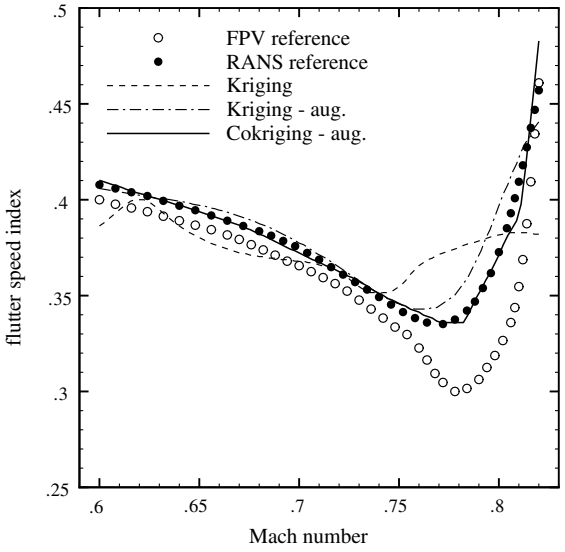

a) Critical flutter speed index

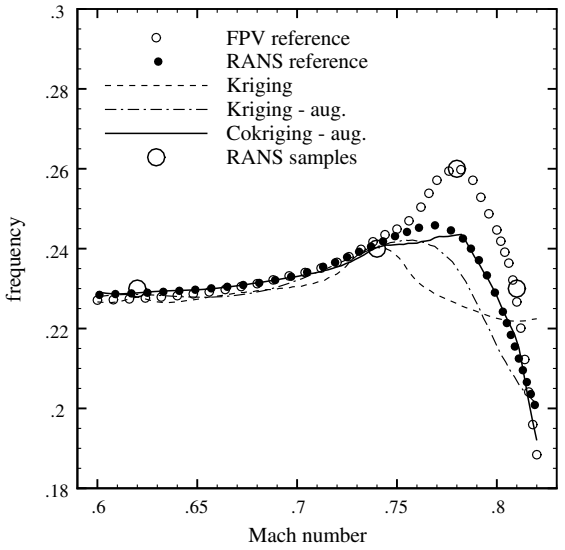

b) Critical response frequency

Fig. 10 Direct kriging and cokriging applied to NACA 0012 aerofoil configuration.

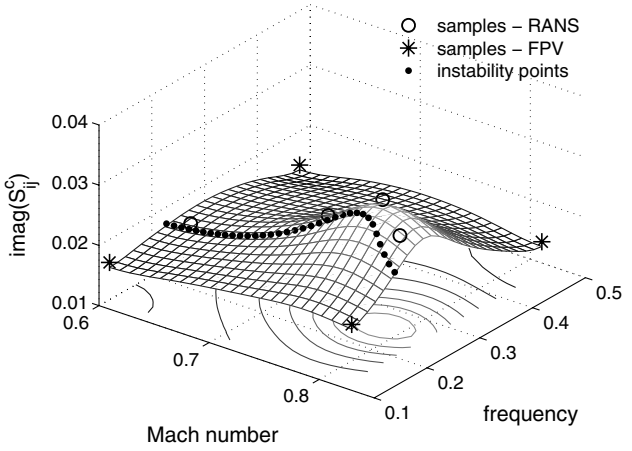

a) Approximated element imag (S^c_{33}) based on direct kriging

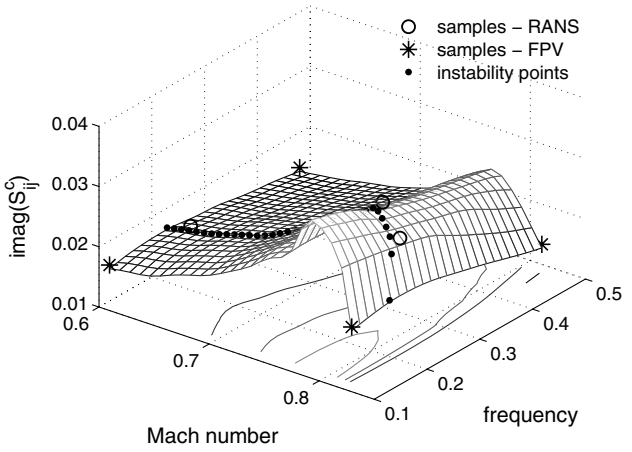

b) Approximated element imag (S^c_{33}) based on cokriging

Fig. 11 Direct kriging and cokriging applied to NACA 0012 aerofoil configuration using augmented sample set.

There is another interesting aspect to kriging, allowing a focused search for a functional extremum following the efficient global optimization (EGO) algorithm, as first presented in [40]. Kriging interpolation provides the prediction of a function, its gradient, and a corresponding standard error, where the prediction and the error can be interpreted to define a normally distributed random variable with mean and standard deviation. While, with the EGO algorithm, an extremum of a function is found by maximizing the so-called EI (applying the normally distributed variable), we are not interested in locating extrema in elements of the interaction matrix itself but to predict the instability, specifically the minimum often relating to the transonic dip or the minimum distance to a proposed flight envelope. Thus, the (assumed) normally distributed kriging prediction of the interaction matrix needs to be propagated to the instability results (i.e., critical values of flutter speed index and response frequency) as described next. For more details about EGO and EI, the reader is referred to [40].

To propagate the error in the kriging approximation, expand the interaction term in Eq. (4) in a Taylor series about the mean critical frequency ω_0 at fixed freestream Mach number M_r,

$$S \approx A_{ss} + \mathcal{N}[\hat{S}^c(\omega_0), \varphi^2(\omega_0)] + \frac{\partial \hat{S}^c(\omega_0)}{\partial \omega_0}(\omega - \omega_0) \qquad (8)$$

where $\mathcal{N}$ denotes the normal distribution. The matrix φ contains the error of the kriging prediction with the square taken elementwise, while the derivative of the interaction term is readily available from the kriging model. A Monte Carlo simulation for random realizations of the normal distribution is done to propagate to the instability prediction, and the EI function is used to locate the minimum value. To obtain the EI for the evaluated critical flutter speed, write $E[\max(V_F^- - Y(M_r), 0)]$, where the operator E denotes the expectation, V_F^- is the current minimum value of the instability prediction, and $Y(M_r) = \mathcal{N}(V_F, \sigma^2)$ is the probability distribution in the critical flutter speed index at a fixed freestream Mach number.

The approach, referred to as EI sampling, is illustrated in Fig. 9. Using intermediate stability results in finding new sample points (as done for risk-based sampling), the samples gather around the converged flutter solution, as seen in Fig. 9a. However, it is obvious that more samples are placed in the region of the transonic dip, since detecting the minimum in the flutter speed is the objective of the EI sampling discussed. This is desirable, because more emphasis is consequently put on the nonlinear transonic regime rather than on the subsonic range. In Fig. 9b, nine samples are sufficient to accurately detect and predict the transonic dip.

The figure also includes (scaled) probability density functions for the critical flutter speed at three freestream Mach numbers for calculations based on 12 samples. Looking at the density function with the highest standard deviation, the idea of EI is nicely described. Risk-based sampling would place a new sample where the standard deviation (i.e., the kriging error) is highest, which is around Mach 0.7. Since the tail of the density function does not suggest an improvement in locating the minimum value of the critical flutter

speed index (i.e., the probability to have a new minimum is very small), EI sampling ignores this location as a possible newly sampled point. EI sampling is more expensive in finding a new sample location, since a probability distribution in flutter speed has to be evaluated for the range of Mach numbers. This cost, however, is insignificant compared with applying the CFD solver.

B. Exploiting Model Hierarchy

Following the preceding discussion, an appropriate sampling reduces the cost considerably in detecting the stability limit for an unknown configuration. The approach can be taken a step further. As mentioned before, the flow models of different fidelity, chosen in this study, usually predict similar response features (as described by the Schur interaction term). In this sense, for instance, a response obtained by a FPV flow model is correlated with a RANS prediction, as changes in a system parameter cause similar changes in the interaction matrix, as illustrated in Fig. 2. Of course, the fundamental assumptions of both the unsteady FP equations and the integral boundary-layer model would hinder an accurate prediction compared with RANS modeling. However, the predictive relationship can still be exploited, as discussed next.

To start with, a blind search using the expensive high-fidelity model is avoided. The initial analysis using a cheaper model delimits the search space for aeroelastic instability and creates a general picture for a configuration. In addition, a relationship for the critical frequency in dependence on the freestream Mach number can be given (for the analysis as described in this paper). This allows the placement of a few carefully selected high-fidelity samples in presumed critical regions, as predicted by the cheaper model.

Figures 10 and 11 present an analysis exploiting the aerodynamic modeling hierarchy. The lower-fidelity model is established by the FPV flow model, whereas the RANS equations are used for higher fidelity. In Fig. 10, the instability boundary is shown as critical values of flutter speed index and response frequency. The figure further includes the predictions based on three different approaches to the kriging approximation, details of which are discussed next. Correspondingly, in Fig. 11, one element of the interaction matrix is given for two of these different kriging approximations. A set of four RANS samples, selected according to the FPV prediction, is used with the sample distribution given in Figs. 10b and 11. Extracting all FPV samples shown in Fig. 2 in the frequency domain is less expensive than evaluating a small number of RANS samples in the time domain.

First, a kriging model based on these four samples was used and, as the results in Fig. 10 demonstrate, the small number of samples and their distribution are inadequate for an accurate prediction. The sample distribution in the frequency/Mach number parameter space along the instability boundary almost gives one-dimensional dependence on the Mach number with little change in the direction of frequency. This significantly complicates the construction of the kriging model with two input dimensions. Thus, it was found to be useful to augment the set of high-fidelity samples by the lower-fidelity corner points. This assumes the initial search space to be big enough to support the kriging model in the frequency dimension but not to adversely effect the approximation close to the instability. Then, a second kriging model, labeled "Kriging-aug.", based on the augmented data is formed. The resulting prediction shows a far better agreement compared with the reference solution.

Finally, cokriging is used, treating the lower-fidelity response as a correlated variable to the higher-fidelity prediction. The input parameter space of the RANS samples is extended by the FPV response, as given in Fig. 2. This means, besides the dependence on response frequency and freestream Mach number, the approximation of the RANS response also depends on the FPV response providing the trend information. Comparing Fig. 2h with Fig. 11b, it is found that the response surface of the presented interaction element is well reproduced. Correspondingly, an accurate prediction of the instability boundary is found in Fig. 10. It is remarked, as seen in the previous paragraph, that even a kriging model based on the augmented data gives good results. This corresponds to the earlier observation from risk-based sampling, where an accurate reconstruction close to the instability (as given by the RANS samples) is essential for the stability prediction.

VI. Conclusions

The approach presented in this paper exploits the formulation of the Schur complement eigenvalue framework and builds an approximation for the interaction term of the Schur matrix. For the approximation, samples of the unsimplified response from a hierarchy of flow models are interpolated using kriging. The kriging approximation approach is analyzed when applied to the structural model of a pitch and plunge aerofoil. Ideas to reduce the cost in constructing the approximation model are discussed. Here, a posteriori risk-based sampling is tested for parametric instability searches, while an aerodynamic model hierarchy is exploited for data fusion and model updating.

While the original Schur eigenvalue method, relying on steady-state simulations and time linearization, is faster than common nonlinear time-accurate approaches, the approximation model proves to be computationally more efficient than the basic formulation, despite the cost spent in the construction of the kriging model itself. Evaluating samples of the Schur interaction matrix at discrete parameter locations, and interpolating, is less expensive than directly using the full formulation, particularly when a space of system parameters is to be investigated for instability. Competitive results are obtained. Another convenient aspect of the proposed method is the access to a hierarchy of (nonlinear) flow models in the aeroelastic stability analysis.

While, in this paper, the approach has been discussed for two-degree-of-freedom aerofoils, the approach is being extended to accommodate more realistic test cases using a modal representation of the structure. In addition, the feasible dimensionality of the parametric problem (i.e., the number of independent parameters) to allow robust and accurate reconstruction and searches is being investigated. This would allow different effects, such as static aeroelastic deformation and, possibly, even structural parameters to be included.

Acknowledgment

This research has been supported by the European Union for the Marie Curie Excellence Team (ECERTA) under contract MEXT-CT-2006-042383.

References

[1] Friswell, M. I., and Mottershead, J. E., *Finite Element Model Updating in Structural Dynamics*, Kluwer Academic, Dorndrecht, The Netherlands, 1995.

[2] Palacios, R., Climent, H., Karlsson, A., and Winzell, B., "Assessment of Strategies for Correcting Linear Unsteady Aerodynamics Using CFD or Experimental Results," *Progress in Computational Flow-Structure Interaction*, edited by W. Haase, V. Selmin, and B. Winzell, Springer–Verlag, New York, 2003, pp. 209–224.

[3] Bhatia, K. G., "Airplane Aeroelasticity: Practice and Potential," *Journal of Aircraft*, Vol. 40, No. 6, 2003, pp. 1010–1018. doi:10.2514/2.7210

[4] Yurkovich, R. N., "Status of Unsteady Aerodynamic Prediction for Flutter of High-Performance Aircraft," *Journal of Aircraft*, Vol. 40, No. 5, 2003, pp. 832–842. doi:10.2514/2.6874

[5] Dowell, E. H., Thomas, J. P., Hall, K. C., and Denegri, C. M., Jr., "Theoretical Predictions of F-16 Fighter Limit Cycle Oscillations for Flight Flutter Testing," *Journal of Aircraft*, Vol. 46, No. 5, 2009, pp. 1667–1672. doi:10.2514/1.42352

[6] Beran, P. S., Khot, N. S., Eastep, F. E., Snyder, R. D., and Zweber, J. V., "Numerical Analysis of Store-Induced Limit-Cycle Oscillation," *Journal of Aircraft*, Vol. 41, No. 6, 2004, pp. 1315–1326. doi:10.2514/1.404

[7] Farhat, C., Geuzaine, P., and Brown, G., "Application of a Three-Field Nonlinear Fluid–Structure Formulation to the Prediction of the Aeroelastic Parameters of an F-16 Fighter," *Computers and Fluids*, Vol. 32, No. 1, 2003, pp. 3–29.

doi:10.1016/S0045-7930(01)00104-9

[8] Woodgate, M. A., Badcock, K. J., Rampurawala, A. M., Richards, B. R., Nardini, D., and deC Henshaw, M. J., "Aeroelastic Calculations for the Hawk Aircraft Using the Euler Equations," *AIAA Journal*, Vol. 42, No. 4, 2005, pp. 1005–1012. doi:10.2514/1.5608

[9] Lucia, D. J., Beran, P. S., and Silva, W. A., "Reduced-Order Modeling: New Approaches for Computational Physics," *Progress in Aerospace Sciences*, Vol. 40, Nos. 1–2, 2004, pp. 51–117. doi:10.1016/j.paerosci.2003.12.001

[10] Amsallem, D., and Farhat, C., "Interpolation method for adapting reduced-order models and application to aeroelasticity," *AIAA Journal*, Vol. 46, No. 7, 2008, pp. 1803–1813. doi:10.2514/1.35374

[11] Bui-Thanh, T., Damodaran, M., and Willcox, K., "Proper Orthogonal Decomposition Extensions for Parametric Applications in Transonic Aerodynamics," AIAA Paper 2003–4213, 2003.

[12] Morton, S. A., and Beran, P. S., "Hopf-Bifurcation Analysis of Airfoil Flutter at Transonic Speeds," AIAA Paper 1996-0060, 1996; also *Journal of Aircraft*, Vol. 36, No. 2, 1999, pp. 421–429. doi:10.2514/2.2447

[13] Morton, S. A., and Beran, P. S., "Hopf Bifurcation Analysis Applied to Deforming Airfoils at Transonic Speeds," AIAA Paper 1997-1772, 1997.

[14] Badcock, K. J., Woodgate, M. A., and Richards, B. E., "Hopf Bifurcation Calculations for a Symmetric Airfoil in Transonic Flow," *AIAA Journal*, Vol. 42, No. 5, 2004, pp. 883–892. doi:10.2514/1.9584

[15] Badcock, K. J., Woodgate, M. A., and Richards, B. E., "Direct Aeroelastic Bifurcation Analysis of a Symmetric Wing Based on Euler Equations," *Journal of Aircraft*, Vol. 42, No. 3, 2005, pp. 731–737. doi:10.2514/1.5323

[16] Woodgate, M. A., and Badcock, K. J., "Fast Prediction of Transonic Aeroelastic Stability and Limit Cycles," *AIAA Journal*, Vol. 45, No. 6, 2007, pp. 1370–1381. doi:10.2514/1.25604

[17] Badcock, K. J., and Woodgate, M. A., "Bifurcation Prediction of Large-Order Aeroelastic Models," *AIAA Journal*, Vol. 48, No. 6, 2010, pp. 1037–1046. doi:10.2514/1.40961

[18] Marques, S., Badcock, K. J., Khodaparast, H. H., and Mottershead, J. E., "Transonic Aeroelastic Stability Predictions Under the Influence of Structural Variability," *Journal of Aircraft*, Vol. 47, No. 4, 2010, pp. 1229–1239. doi:10.2514/1.46971

[19] Raj, P., "Computational Uncertainty: Achilles' Heel of Simulation Based Aircraft Design," *AVT-147 Symposium on 'Computational Uncertainty in Military Vehicle Design'*, NATO RTO-MP-AVT-147, 2007.

[20] Badcock, K. J., Richards, B. E., and Woodgate, M. A., "Elements of Computational Fluid Dynamics on Block Structured Grids Using Implicit Solvers," *Progress in Aerospace Sciences*, Vol. 36, Nos. 5–6, 2000, pp. 351–392. doi:10.1016/S0376-0421(00)00005-1

[21] Jameson, A., "Time Dependent Calculations Using Multigrid with Applications to Unsteady Flows Past Airfoils and Wings," AIAA Paper 1991–1596, 1991.

[22] Osher, S., and Chakravarthy, S., "Upwind Schemes and Boundary Conditions with Applications to Euler Equations in General Geometries," *Journal of Computational Physics*, Vol. 50, No. 3, 1983, pp. 447–481. doi:10.1016/0021-9991(83)90106-7

[23] van Leer, B., "Towards the Ultimative Conservative Difference Scheme, V: A Second-Order Sequel to Godunov'S Method," *Journal of Computational Physics*, Vol. 32, No. 1, 1979, pp. 101–136. doi:10.1016/0021-9991(79)90145-1

[24] Menter, F. R., "Zonal Two Equation k-ω Turbulence Models for Aerodynamic Flows," AIAA Paper 1993–2906, 1993.

[25] Timme, S., and Badcock, K. J., "oFPfoil (v1.0): User Guide," Univ. of Liverpool, Computational Fluid Dynamics Lab., Department of Engineering, Liverpool, U.K., 2010, http://cfd4aircraft.com/4downloads.php [retrieved 15 March 2011].

[26] Holst, T. L., "Transonic Flow Computations Using Nonlinear Potential Methods," *Progress in Aerospace Sciences*, Vol. 36, No. 1, 2000, pp. 1–61. doi:10.1016/S0376-0421(99)00010-X

[27] Whitfield, D. L., "Analytical Description of the Complete Turbulent Boundary Layer Velocity Profile," AIAA Paper 1978–1158, 1978.

[28] Whitfield, D. L., Swafford, T. W., and Jacocks, J. L., "Calculation of Turbulent Boundary Layers with Separation and Viscous–Inviscid Interaction," *AIAA Journal*, Vol. 19, No. 10, 1981, pp. 1315–1322. doi:10.2514/3.60066

[29] Swafford, T. W., "Analytical Approximation of Two-Dimensional Separated Turbulent Boundary Layers," *AIAA Journal*, Vol. 21, No. 6, 1983, pp. 923–926. doi:10.2514/3.8177

[30] Drela, M., and Giles, M. B., "Viscous–Inviscid Analysis of Transonic and Low Reynolds Number Airfoils," *AIAA Journal*, Vol. 25, No. 10, 1987, pp. 1347–1355. doi:10.2514/3.9789

[31] Lighthill, M. J., "On displacement thickness," *Journal of Fluid Mechanics*, Vol. 4, No. 04, 1958, pp. 383–392. doi:10.1017/S0022112058000525

[32] Cook, P. H., McDonald, M. A., and Firmin, M. C. P., "Aerofoil RAE 2822: Pressure Distributions, and Boundary Layer and Wake Measurements," AGARD TR AR 138, 1979.

[33] Fung, Y. C., *An Introduction to the Theory of Aeroelasticity*, Wiley, New York, 1955, pp. 210–212.

[34] Dowell, E. H., Clark, R., Cox, D., Curtiss, H. C., Jr., Edwards, J. W., Hall, K. C., Peters, D. A., Scanlan, R., Simiu, E., Sisto, F., and Strganac, T. W., *A Modern Course in Aeroelasticity*, Kluwer Academic, Dordrecht, The Netherlands, 2004, pp. 60–64.

[35] Davis, T. A., "UMFPACK Version 5.4.0 User Guide," Univ. of Florida, Department of Computer and Information Science and Engineering, TR 04–003 rev., Gainesville, FL, 2009, http://www.cise.ufl.edu/research/sparse/umfpack/ [retrieved 15 March 2011].

[36] Bekas, C., and Saad, Y., "Computation Of Smallest Eigenvalues Using Spectral Schur Complements," *SIAM Journal on Scientific and Statistical Computing*, Vol. 27, No. 2, 2005, pp. 458–481. doi:10.1137/040603528

[37] Hassig, H. J., "An Approximate True Damping Solution of the Flutter Equation by Determinant Iteration," *Journal of Aircraft*, Vol. 8, No. 11, 1971, pp. 885–889. doi:10.2514/3.44311

[38] Brigham, E. O., *The Fast Fourier Transform and its Applications*, Prentice–Hall, Englewood Cliffs, NJ, 1988, pp. 75–77.

[39] Sacks, J., Welch, W. J., Mitchell, T. J., and Wynn, H. P., "Design and Analysis of Computer Experiments," *Statistical Science*, Vol. 4, No. 4, 1989, pp. 409–435. doi:10.1214/ss/1177012413

[40] Jones, D. R., Schonlau, M., and Welch, W. J., "Efficient Global Optimization of Expensive Black-Box Functions," *Journal of Global Optimization*, Vol. 13, No. 4, 1998, pp. 455–492. doi:10.1023/A:1008306431147

[41] Lophaven, S. N., Nielsen, H. B., and Soendergaard, J., "DACE: A Matlab Kriging Toolbox," Technical Univ. of Denmark, TR IMM-TR-2002-12, Lyngby, Denmark, 2002.

[42] Ghoreyshi, M., and Badcock, K. J., "Accelerating the Numerical Generation of Aerodynamic Models for Flight Simulation," *AIAA Journal*, Vol. 46, No. 3, 2009, pp. 972–980. doi:10.2514/1.39626

[43] McKay, M. D., Conover, W. J., and Beckman, R., "A Comparison of Three Methods for Selecting Values of Input Variables in the Analysis of Output from a Computer Code," *Technometrics*, Vol. 21, No. 2, 1979, pp. 239–245. doi:10.2307/1268522

[44] Isogai, K., "Transonic-Dip Mechanism of Flutter of a Sweptback Wing: Part II," *AIAA Journal*, Vol. 19, No. 9, 1981, pp. 1240–1242. doi:10.2514/3.7853

P. Beran
Associate Editor